Scientific paper

Visible-Light Photoactivity of Bi-pyrochlores with High Fe Contents

Matjaz Valant, Metka Bencina and Mattia Fanetti

Materials Research Laboratory, University of Nova Gorica, 5000, Nova Gorica, Slovenia

** Corresponding author: E-mail: matjaz.valant@ung.si*

Received: 06-12-2013

Dedicated to the memory of Prof. Dr. Marija Kosec.

Abstract

Three Bi-pyrochlores with different Fe contents ($Bi_2Ti_2O_7$, $Bi_{1.65}Nb_{1.12}Fe_{1.16}O_7$ and $Bi_{1.9}Te_{0.58}Fe_{1.52}O_{6.87}$) were synthesized in the form of nanopowders with similar morphological characteristics. All three nanopowders show an intensive visible-light photocatalytic activity. The analysis of their band gap and absorption characteristics has shown a strong correlation with the Fe-content indicating that a significant band gap reduction can be obtained by Fe incorporation. The photocatalytic activity has not followed this trend. The initial increase in the Fe-content has resulted in a significant enhancement of the photoactivity while with the further increase the photoactivity has slowly decreased. The reason for this behaviour has been proposed to be in an opposing influence of the increased exciton density and recombination rate.

Keywords: Photoactivity, Bi-pyrochlores, Fe-content

1. Introduction

The quest for an efficient visible-light photocatalyst for organic pollutant decomposition or even water splitting for solar hydrogen production is on the top of the list of environmental technologies for future sustainable growth. At the moment, harvesting of the solar light for these processes is of low efficiency mainly due to material science problems. The current photocatalysts are compromising between, on the one hand, large band gaps that enable absorption of only UV light but also provides a high reduction potential and photochemical stability and, on the other hand, visible-light absorbing smaller band gaps with less electron potential and higher photocorrosion. Another important characteristic is an electron recombination rate that mainly depends on electron lifetime, crystallinity and purity of the materials. As the UV light represents only about 5% of the solar light energy the efficiency of the UV photocatalysts is very limited. The efficiency can be significantly increased if the absorption is extended into the visible-light range. Many different approaches for so-called band gap engineering have been developed by now among them cation and anion doping, formation of solid solution, Z-scheme etc.

Our research approach has focused on chemical design of crystal structures that can tolerate a versatile range of different metal ions. A family of such compounds are pyrochlores. The ideal structural arrangement of the pyrochlore with $Fd\bar{3}m$ cubic symmetry consists of A and B metal ions that occupy *16d* (0.5, 0.5, 0.5) and *16c* (0, 0, 0) special positions, respectively, whereas O and O' atoms occupy non-equivalent crystallographic sites *48f* (x, 0.125, 0.125) and *8b* (0.375, 0.375, 0.375), respectively. In the pyrochlore $A_2B_2O_7$ structure, A_2O' chains weakly interact with the more rigid B_2O_6 network. Therefore, cation and/or anion vacancies in the A_2O' network of defect pyrochlores do not significantly reduce the stability of the lattice. In the Bi-based pyrochlores, a positional disorder in the A_2O' is often encountered.[1,2] It is attributed to the stereochemically active Bi6s lone electron pair.[3] (Fig. 1)

For the development of the visible light photocatalysts we have focused on the research of Bi-containing pyrochlores. The reason for this choice is that *Bi6s* orbital hybridizes with *O2p* orbital, which efficiently increases the band edge of the valence band and, consequently, decreases the band gap.[4] The most investigated member of this kind is $Bi_2Ti_2O_7$, for which the DFT modelling has shown a rather complex electron band structure with possible concurrent indirect and direct electron transitions

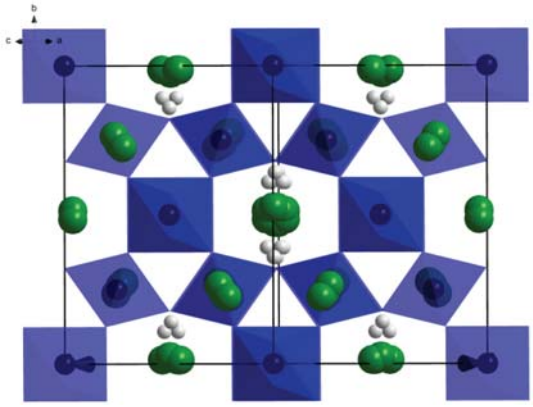

Fig. 1: Crystal structure of the BTF pyrochlore projected close to (110) direction. The blue corner-connected octahedra represent $(Fe,Te)_2O_6$ substructure (A_2O_6 sites). The green toroids represent six equivalent (Bi,Fe) sites and grey spheres represent O atoms on the positionally disordered A_2O' sites.

over the band gaps of 2.46 eV and 2.89 eV, respectively.[5] Experimental work on $Bi_2Ti_2O_7$ has confirmed its photoactivity in visible light region.[6,7]

We have further narrowed down the range of the interesting pyrochlores with a requirement that they must contain Fe ions. Fe ions have been shown to decrease the band gap by formation of interband states due to the localized orbitals of *3d* metals.[8] The interband states couple with either conductive or valence band, which effectively leads to the band gap reduction. The beneficial influence of the Fe ions on the photoactivity in UV range has been shown for Bi_2FeTaO_7 and Bi_2FeNbO_7 pyrochlores.[9–11] The rather coarse agglomerates of the micron size powders have not been tested for visible-light photoactivity but in the UV range they have shown a similarly high photoactivity as the TiO_2 references and higher than members of the same pyrochlore family without Fe. Doping of $Bi_2Ti_2O_7$ with Fe has also shown significant increase in photoactivity.[12] In this study an attempt has been made to describe the influence of Fe content to the photoactivity; however, the authors has not been able to produce the single phase Fe-doped $Bi_2Ti_2O_7$ powder with more than 1% Fe. For this reason it remains unclear why they have experienced a significant reduction in the photoactivity for the higher nominal Fe contents.

Recently, an intensive visible-light photocatalytic activity has been shown for the Bi-Fe-Nb pyrochlore nanoparticles.[13] The nanoparticles with $Bi_{1.65}Nb_{1.12}Fe_{1.16}O_7$ composition (BNF) and a size of about 40 nm showed the indirect and direct band gaps of 1.90 eV and 2.60 eV, respectively. This is reflected in light absorption up to 650 nm, which is a prerequisite for the observed visible-light photoactivity. Parallel photocatalytic tests have shown that this Fe-containing pyrochlore significantly exceeds the photoactivity of similar $Bi_2Ti_2O_7$ (BT) nanoparticles. Certainly, the enhancement in the photoactivity can be attributed to the narrower band gap of the BNF pyrochlore. However, it is well known that Fe ions also introduce adverse effects such as an increase in the recombination rate.[14] For instance, in hematite the electron–hole recombination occurs on picoseconds to milliseconds timescale,[15,16] while the hole diffusion lengths is as short as 2–20 nm.[17,18] The adverse influence of enhanced recombination can be somewhat suppressed by using nanosize particles, for which the size is less than the diffusion range of the minor carriers.

In this work we have investigated the influence of the Fe-content in Bi-pyrochlore nanoparticles on their photocatalytic activity. The studies are expected to answer the question whether the Fe-content in the pyrochlores can be positively correlated to the increase in the photocatalytic activity or adverse influences, such as the increased recombination, prevail. In addition to the reports on BT and BNF,[8] we present here an investigation on yet another member of this line of pyrochlores with even higher Fe-content. To further increase the Fe amount in the pyrochlore Fe^{3+} ions on the B-site should be combined with even higher formal charged ions such as Te^{6+}. The Bi-Fe-Te pyrochlore (BTF) is a pyrochlore with so far the highest known amount of Fe and as such suitable for this study. It has recently been synthesized in the bulk form.[19] The compositional range of the pyrochlore phase has been shown to be $(Bi_{2-x}Fe_x)(Fe_{1.42}Te_{0.58})O_{6.87}$. In the bulk form it was characterized as a narrow band gap semiconductor with an indirect band gap of 1.965 eV.[20] The first challenge of this study is to synthesize the nanoparticles of this ternary compound, crystallize them and disperse in the water. The photocatalytic characterization will then be performed on BT, BNF and BTF pyrochlore systems with similar morphologic characteristics in order to reduce the number of variables that may influence the photoactivity. The obtained results will be discussed in correlation to the Fe content in the pyrochlores.

2. Experimental

BTF nanoparticles were synthesized with co-precipitation method. Stoichiometric amounts of bismuth(III) nitrate pentahydrate (Alfa Aesar, 98%), iron(III) nitrate nonahydrate (Alfa Aesar, 98+%) and Te powder (60 mesh, Alfa Aesar, 99.999%) were used as precursor materials. Bismuth nitrate, iron nitrate and Te powder were dissolved in 25 mL of nitric acid (Fluka, 65%). The obtained solution was stirred for 1 h and treated with ammonia aqueous solution. The ammonia solution was added very slowly, drop by drop, until the pH reached 8. A pale orange precipitate was filtered and washed with abundant of deionized water with intermediate centrifuging for several times. The powder was then dried at 100 °C for approximately 2 h. The synthesized powder was annealed in the furnace at 570 °C for 7 h in an aluminium oxide crucible in air. Heating and cooling rates were ≈ 8 °C/min. The synthesis of BT and BNF nanoparticles has been performed as described in Ref. 11.

The structural analysis was performed by X-ray powder diffraction technique (XRD) using PANalytical X'pert pro MPD instrument with Cu K-alpha radiation over the 2Θ range 5° to 90°, with a step size of 0.017°, divergence slit of 0.218° and counting step time of 25 s in continuous scanning mode. The morphological analysis was performed by a scanning electron microscope (JEOL FEG SEM, JSM 7100F TTLS). The energy dispersive X-ray analysis (Oxford EDX, XMAX 80mm^2) analysis performed on the same microscope showed the BTF composition to be $Bi_{1.9}Te_{0.58}Fe_{1.52}O_{6.87}$. UV-Vis spectrophotometer with integrating sphere was used to measure the diffuse reflectance spectra of powders. Dynamic light scattering (DLS, NanoBrook 90Plus) analysis has been used to determine the size of agglomerates. The absorption data of the synthesized materials was determined by Kubelka Munk function. The band gap energy was estimated as the intersection between the linear fit of absorbance plot and the photon energy axis.

The photocatalytic activity was evaluated by degradation of methyl orange (MO – Alfa Aesar, ACS) using a custom-made photoreactor, built from four 60 W lamps that emit only light with the wavelengths above 410 nm and thus allowing selectively testing in the visible spectral range. The photoreactor walls were made from highly reflective Al-foil to retain high luminous efficacy. Under the water-cooled 100 mL cell a magnetic stirrer was placed in order to maintain the reaction mixture homogenous. The photocatalyst (0.1 g) was suspended in 75 mL of MO solution with an initial dye concentration of 7 mg/l. Prior to irradiation the samples were ultrasonicated for 30 s in order to disperse the nanoparticles. All the photocatalytic activity tests were performed with the addition of 4 mL of H_2O_2 (Belinka Perkemija, 30%) added to the photocatalyst solution after the ultrasonication. The photocatalyst solution with pH of 4 was kept at ~12 °C. The first sample was removed from the suspension at the start of irradiation and this was considered as the initial concentration, C_0. The mixture was stirred during irradiation. At given time intervals, aliquots (4 mL) were taken out from the suspension by a syringe and centrifuged for 15 min at 10000 rpm in order to remove photocatalyst particles. The absorption maximum at 464 nm was monitored with a Perkin Elmer Lambda 650s spectrophotometer. The blank experiment without photocatalyst was performed under the same conditions.

3. Results

The samples for the present study were prepared in the nanopowder form, for which the visible-light photoactivity has been shown. It is important that the size of the prepared nanoparticles and their agglomerates is similar in order to exhibit similar active surface area. In addition, to reliably compare their photocatalytic properties the nanopowders should also be well crystallized. All these pa-

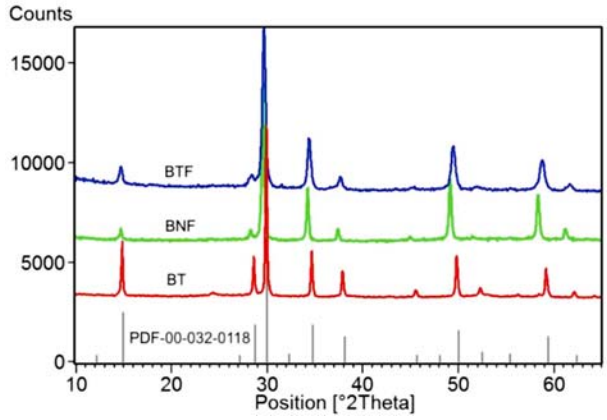

Fig. 2: XRD pattern of the synthesized BT, BNF and BTF pyrochlores nanoparticles

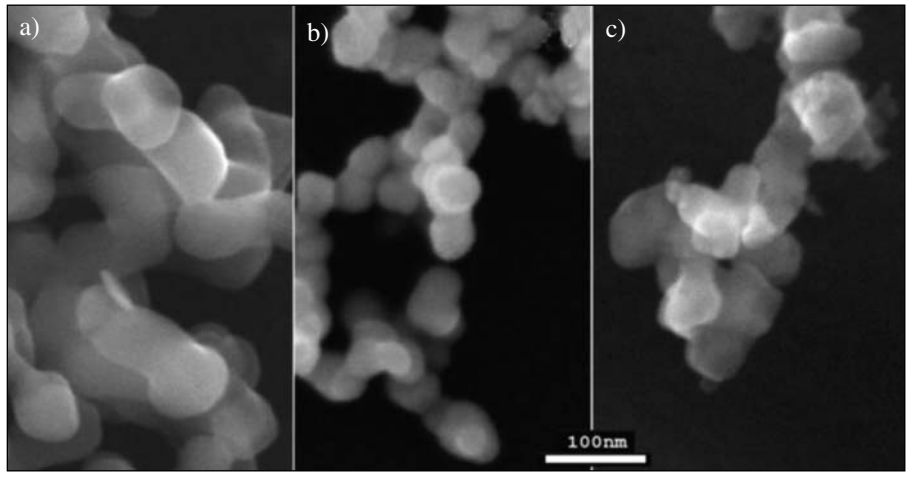

Fig. 3: SEM images of the synthesized (a) BT, (b) BNF and (c) BTF nanoparticles showing the size of the crystallites and their agglomeration. All images are shown with the same scale.

rameters have been carefully analyzed and determined. Fig. 2 shows the XRD patterns of the synthesized BT, BNF and BTF pyrochlores. From the XRD patterns we can see that the powders are well-crystallized single-phase pyrochlores with a comparable line broadening. The crystallite size has been determined by Scherrer's equation and from SEM imaging (Fig. 3). With both techniques the size of the particles has been found to be similar, in the range from 40 nm (BNF) to 70nm (BT). The detail values are given in Table I. Further, DLS has been used to measure the size of agglomerates. It has been shown that the powders are only lightly agglomerated. The BTF agglomerates were found to be somewhat bigger; however, they all have been in the range from about 200–300nm.

The absorption spectra, transformed from the UV-vis diffuse reflectance by the Kubelka-Munk function (Fig. 4),[21] show that the light absorption of BTF and BNF extends much farther into the visible range than the absorption of BT. The BTF nanoparticles can absorb light with a wavelength as high as ~650 nm. The high absorbance of BTF is in accordance with the narrowest band gap among the tested pyrochlores. The band gap energy (E_g) of BTF nanoparticles was estimated from the linear extrapolations of $[F(R) \cdot hv]^{1/2}$ and $[F(R) \cdot hv]^2$ vs. hv for the indirect and direct band gap transition of electrons and found to be 1.75 eV and 2.56 eV, respectively (Fig. 5, Table I).

The photocatalytic activity of the synthesized powders, evaluated by the degradation of the MO solution, is the lowest for the BT nanoparticles (Fig. 6). After 4 h of visible light irradiation only about 40% degradation has been obtained. The BNF particles have shown much higher photoactivity with almost complete degradation after 4 h treatment. Interestingly, the BTF nanoparticles have not given any better degradation as it would be expectetd from their better absorption characteristics. They have even shown slightly slower kinetics of degradation. After 4 h of irradiation 7 % less MO was degraded than with BNF nanoparticles.

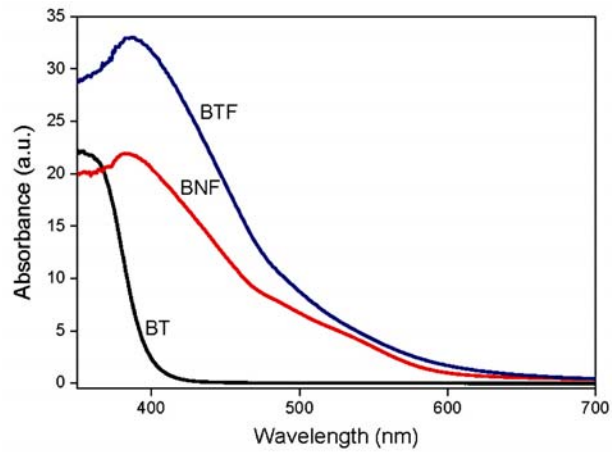

Fig. 4: UV-visible absorbance spectra of BT, BNF and BTF

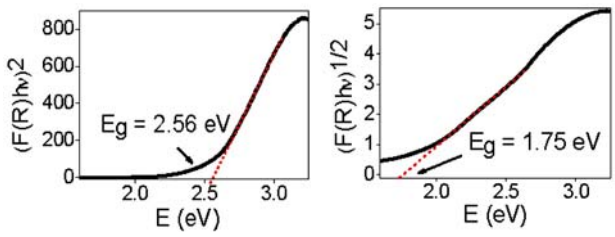

Fig. 5: Band gap energy of BTF, calculated by the Kubelka-Munk function,[21] for (a) direct and (b) indirect transition of electrons

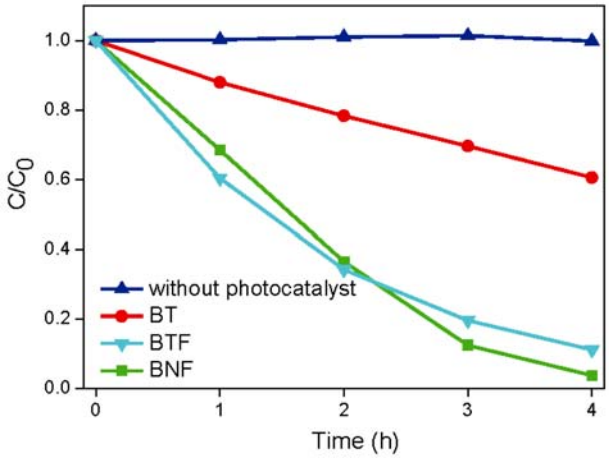

Fig. 6: Visible-light photocatalytic degradation of methyl orange without any photocatalysts and with BT, BNF and BTF nanopowder (all in presence of the H_2O_2 scavenger)

4. Discussion

The three tested pyrochlore nanopowders of a similar particle size show variations in the band gap proper-

Table I: Comparison of the measured parameters for the synthesized BT, BNF and BTF nanopowders with respect to their Fe content

Compound	Fe-content (at% of metal)	Degradation rate of MO (%) (after 4h)	E_g (eV) indirect/direct	Crystallite size (nm)	Mean diameter by DLS (nm)
$Bi_2Ti_2O_7$ – (BT)	0	0.40	2.46 / 3.18	70	≈ 250
$Bi_{1.65}Nb_{1.12}Fe_{1.16}O_7$ – (BNF)	29.5	0.96	1.90 / 2.60	40	≈ 200
$Bi_{1.9}Te_{0.58}Fe_{1.52}O_{6.87}$ – (BTF)	38.0	0.89	1.75 / 2.56	50	≈ 300

ties, which trends are in accordance with the current understanding of the influence of Fe electrons on the electronic structure of oxide semiconductors. With an increase in Fe content the band gap of the pyrochlores becomes narrower as a consequence of an increased density of the interband states coupled to either valence or conduction band. The determined absorption characteristics of the pyrochlores follow this trend, so that BTF with the highest Fe content absorbs up to the highest wavelengths of the visible light spectrum. During the illumination with the visible light this induces the highest density of excitons that potentially can be involved in the photocatalytic reaction. Based on this it would be expected that the photoactivity of BTF would exceed the one of BNT. We have been able to confirm the visible-light photoactivity of BTF but the intensity is, surprisingly, very similar (or even smaller) than that of BNT.

Clearly, the electron and hole potential of BTF is suitable for the decomposition of MO (with assistance of H_2O_2 scavenger). However, the most intensive light absorption is not reflected in the most intensive photoactivity. These results indicate that some adverse processes, related to the presence of Fe, must exist and prevail at some critical Fe concentrations. It is reasonable to assume that the adverse processes are related to an increase in the electronic recombination rate. This reduces the yield of the excited carriers that can cross the solid-liquid interface and get involved in the chemical reaction. At the critical Fe concentration the recombination becomes so intensive that it annihilates the increase in the exciton density due to stronger light absorption. The high recombination rate in Fe-containing semiconductors have already been described for Fe_2O_3[14–18] so it makes no surprise that the same processes are also introduced by Fe into other host crystal lattices.

5. Conclusions

We have shown that, contrary to their bulk analogues, all tested pyrochlore nanopowders exhibit quite intensive visible light photocatalytic activity. Band gap energy of Bi-pyrochlores can be significantly decreased by introduction of Fe into the crystal lattice. However, the decrease in the band gap energy is not reflected in the increase in the photocatalytic activity. The Fe-containing Bi-pyrochlores indeed exhibit much higher photocatalytic activity than $Bi_2Ti_2O_7$. However, at the high Fe concentration the adverse processes, like an increase in recombination rate, start to prevail over the increase in the absorption. We have shown that for such compounds the photocatalytic activity decreases.

6. References

1. M. W. Lufaso, T. A. Vanderah, I. M. Pazos, I. Levin, R. S. Roth, J. C. Nino, V. Provenzano, P. K. Schenck, *J. Sol. St. Chem.* **2006**, *179*, 3900–3910.
2. I. Levin, T. G. Amos, J. C. Nino, T. A. Vanderah, C. A. Randall, M. T. Lanagan, *J. Sol. St. Chem.* **2002**, *168*, 69–75
3. M.Avdeev, M. K.Haas, J. D. Jorgensen, R. J. Cava, *J. Sol. St. Chem.* **2002**, *169*, 24–34
4. R. Shi, J. Lin, Y. Wang, J. Xu, Y. Zhu, *J. Phys. Chem. C.* **2010**, *114*, 6472–6477
5. W. Wei, Y. Dai, B. Huang, *Phys. Chem.C* **2009**, *113*, 5658–5663
6. J. Hou, S. Jiao, H. Zhu, R.V. Kumar, J. Solid State Chem. 2011, 184, 154–158
7. S. Murugesan, V. R. Subramanian, *Chem. Commun.* **2009**, *34*, 5109–5111
8. S. Murugesan, M. N. Huda, Y. Yan, M. M. Al-Jassim, V. Subramanian, J. *Phys. Chem.* C. **2010**, *114*, 10598–10605
9. L. L. Garza-Tovar, L. M. Torres-Martinez, D. B. Rodriguez, R. Gomez, G. del Angel, *J. Mol. Cat. A: Chemical* **2006,** *247*, 283–290
10. L. M. Torres-Martinez, I. Juarez-Ramirez, J. S. Ramoz-Garza, F. Vazquez-Acosta, S. W. Lee, *WSEAS Transactions on Environment and Development*. **2010**, *6*, 286–295
11. K.L. Rosas-Barrera, J.L. Ropero-Vega, J.A. Pedraza-Avella, M.E. Nino-Gomez, J.E. Pedraza-Rosas, D.A. Laverde-Catano, *Catalysis Today* **2011,** *166*, 135–139
12. B. Allured, S. DelaCruz, T. Darling, M. N. Huda, V. Subramanian, *Applied Catalysis B: Environmental* **2014,** *144,* 261–268.
13. M. Bencina, M. Valant, M. W. Pitcher, M. Fanetti, *Nanoscale* **2014**, DOI: 10.1039/C3NR04260J
14. M. Barroso, S. R. Pendlebury, A. J. Cowan, J. R. Durrant, *Chem. Sci.* **2013**, *4*, 2724–2734
15. R. Pendlebury, M. Barroso, A. J. Cowan, K. Sivula, J. W. Tang, M. Grätzel, D. Klug, J. R. Durrant, *Chem. Commun*. **2011**, *47*, 716–718
16. Z. Q. Huang, Y. J. Lin, X. Xiang, W. Rodriguez-Cordoba, K. J. McDonald, K. S. Hagen, K. S. Choi, B. S. Brunschwig, D. G. Musaev, C. L. Hill, D. W. Wang, T. Q. Lian, *Energy Environ. Sci*. **2012**, *5*, 8923–8926
17. J. H. Kennedy, K. W. Frese, J. Electrochem. Soc. 1978, 125, 709–714
18. M. P. Dare-Edwards, J. B. Goodenough, A. Hamnett, P. R. Trevellick, *J. Chem. Soc., Faraday Trans.* **1983**, *79,* 2027–2041
19. G. S. Babu, M. Valant, K Page, A. LLobet, T. Kolodiazhnyi, A. K. Axelsson, *Chem. Mater*. **2011**, *23*, 2619–2625
20. M. Valant, G. S. Babu, M. Vrcon, T. Kolodiazhnyi, A.-K. Axelsson, *J. Am. Ceram. Soc.* **2012***, 95*, 644–650
21. P. Kubelka, F. Munk. *Zeitschrif. Techn. Physik* **1931**, *12*, 593–601.

Povzetek

Sintetizirali smo tri materiale s piroklorno strukturo z različno vsebnostjo Fe ($Bi_2Ti_2O_7$, $Bi_{1.65}Nb_{1.12}Fe_{1.16}O_7$ in $Bi_{1.9}Te_{0.58}Fe_{1.52}O_{6.87}$) v obliki nanodelcev in s podobnimi morfološkimi lastnostmi. Vsi trije materiali kažejo intenzivno fotoaktivnost pod vidno svetlobo. Analiza energije prepovedanih pasov in absoropcijske karakteristike materialov so pokazale močno povezavo z vsebnostjo Fe v materialih, saj se z vključitvijo Fe ionov v kristalno mrežo prepovedan pas materiala zelo zmanjša. Nasprotno pa fotokatalitska aktivnost ne sledi temu trendu. S prvotnim povečanjem vsebnosti Fe se je fotoaktivnost zelo povečala, medtem ko je nadaljnje povečanje povzročilo rahlo zmanjšano fotokaktivnost. Razlog za takšno obnašanje bi lahko bila povečana gostota excitonov in večja stopnja rekombinacije.